International Journal of Science and Engineering Invention (IJSEI)
Volume 09, October 2023,
https://doi.org/10.23958/ijsei/vol09-i10/258

Original article

Entropy Generation Analysis for a Transient Micropolar Thermofluidics: Numerical Strategy

Paresh Vyas, Manvi Adha *

Department of Mathematics, University of Rajasthan, Jaipur.

*Corresponding author: Manvi Adha; *manvi.maths11@gmail.com*

Received 03 September 2023; Accepted 30 September 2023; Published 12 October 2023

Abstract

In this communication, A numerical solution strategy has been devised to compute entropy in a thermo-fluidic system comprising micropolar fluid in a Darcian regime bounded by a vertically moving plate experiencing time-dependent suction. The Crank- Nicolson numerical scheme exploited to solve the governing equations results in a tri-diagonal block matrix system. The resultant system is then solved by the Thomas algorithm, which provides pertinent quantities of interest. The velocity and thermal fields are used to compute entropy generation. The profiles for entropy generation and Bejan number are portrayed and discussed.

Keywords: ***Micropolar fluid, Porous medium, Entropy.***

Introduction

Entropy aspects in thermo-fluidic systems are pertinent for energy optimization in engineering systems. It is physically realized that real fluidic systems confront thermodynamic irreversibility, which causes energy losses due to heat transfer, dissipation, magnetic field, radiation, walls of a porous medium, etc. Bejan [1,2] showed that irreversibility analysis of fluidic systems facilitates parametric study that allows the identification of parameters impacting entropy generation. We can select parameters wisely that help reduce entropy without compromising the design. Realizing the importance of entropy analysis in thermo fluidic systems and interesting applications, numerous authors have focused on fluidic systems for second law analysis aspects. These studies varied in terms of choice of fluids, geometries and allied features. Rashidi et al. [3] investigated entropy generation in steady MHD flow due to a rotating porous disk in a nanofluid. Maougal and Bessaïh [4] studied heat transfer and entropy analysis for mixed convection in a discretely heated porous square cavity. Vyas and Srivastava [5] performed entropy analysis for a flow inside a composite duct with asymmetric convective cooling. Matin [6] analysed entropy generation in combined heat and mass transfer over a plate embedded in a porous medium. Vyas and Khan [7] considered MHD dissipative Casson fluid flow for Entropy analysis. Srivastava et al. [8] trapped entropy in a vertical channel, facilitating oscillatory flow. Vyas and Soni [9] analysed entropy in a unique boundary layer flow due to a point sink at the cone's vertex. Kumari and Raju [10] investigated time-dependent MHD free convective flow past a vertical porous plate with fluctuating heat and mass transfer effects. Vyas et al. [11] conducted a numerical analysis of entropy encountered in Micropolar fluid flow under boundary layer assumptions. Vyas and Yadav [12] analysed entropy for a convective regime over a vertical stretching cylinder. Monaledi and Makinde [13] simulated entropy for microchannel nanofluid flow. Egunjobi and Makinde [14] examined entropy in nano-liquid film over an inclined heated surface. Vyas and Khan [15] investigated entropy in micropolar couple stress fluid flow in the Forchheimer channel.

The Micropolar fluid has microstructures characterized by additional internal degrees of freedom. Due to its unique properties, it has found numerous applications in various industrial processes such as lubrication, coating, and heat transfer. The studies of micropolar fluids have wide applications in various technological processes in chemical, pharmaceutical, and food industries. These include the polymer industry, liquid crystals, lubricant formulation, colloidal suspensions, etc. As far as the mathematical description of such fluids is concerned, it is noticed that the classical Navier-Stokes theory needs refinement. Constitutive equations for Newtonian fluids should be extended to address more complex fluids with microstructures exhibiting micro-rotational effects and supporting surface and body couples. Eringen [16,17] developed the theory of micro fluids, including the effect of local rotary inertia, the couple stress and inertial spin. The crux of the theory is that rigid randomly oriented particles contained in a small fluid volume element undertake rotation about the centre of the volume elements described by a microrotation vector.

The flow past a surface is worth studying due to wide theoretical and technological points of view and consequently received attention. Soundalgekar and Takhar [18] discussed micropolar fluidics past a continuously moving plate. Gorla et al. [19] examined natural convective micropolar fluid flow over a uniformly heated vertical plate. Kim [20] developed a perturbation solution transient convection of micropolar fluid past a vertical porous plate bounding a porous medium. Srinivasacharya et al. [21] studied the unsteady Stokes flow of micropolar fluid between two parallel porous plates. Kim and Fedorov [22] examined a micropolar fluid's time-dependent mixed radiative convection flow past a moving semi-infinite vertical porous plate. Kim [23] examined mass transfer in MHD micropolar flow over a vertically moving porous plate in a porous medium.

Chaudhary and Jain [24] developed a perturbation scheme for investigating magneto-micropolar fluid flow for heat and mass transfer due to a radiate surface. Abdulaziz and Hashim [25] studied fully developed free convection mass transfer of a micropolar fluid between porous vertical plates. Das [26] studied the effect of chemical reactions and thermal radiation on MHD micropolar fluid's heat and mass transfer flow in a rotating frame of reference. Sharma and Jha [27] studied heat transfer in MHD micropolar fluid flow past a vertical plate in a slip-flow regime. Pal and Talukdar [28] used the perturbation technique to study unsteady MHD mixed convection periodic flow, heat and mass transfer in micropolar fluid with chemical reaction in the presence of thermal radiation. Ashraf et al. [29] studied MHD non-Newtonian micropolar fluid flow and heat transfer in a channel with stretching walls. Narayana et al. [20] investigated the effects of Hall current and radiation absorption on MHD micropolar fluid in a rotating system. Gangadhar et al. [31] investigated the effects of Newtonian heating on micropolar ferrofluid flow past a stretching surface. Magodora et al. [32] investigated dual solutions of a micropolar nanofluid flow with radiative heat mass transfer over a stretching/shrinking sheet using the spectral quasi-linearization method. Ahmad et al. [33] investigated the Cattaneo–Christov heat flux model for stagnation point flow of micropolar nanofluid toward a nonlinear stretching surface with slip effects.

However, the studies reported above, references contained therein and other works have given scanty attention to thermodynamic irreversibility aspects. In this study, we aim to demonstrate the application of a powerful numerical scheme for the setup undertaken herein with central stimuli to trap the features of inherent thermodynamic irreversibility. The study, it is expected, would serve as a tool for further applications. It is not out of place to record that the Crank-Nicolson method is a powerful numerical technique used to solve differential equations that arise in various fields of science and engineering. Its accuracy, stability, efficiency, or a combination of these factors make it a robust numerical solution tool. The findings tabled and portrayed graphically will be discussed at length.

Mathematical model

We consider a steady laminar incompressible micropolar fluid past a flat infinite plate moving vertically upwards embedded in a fluid-saturated porous medium. A plate bearing a uniform temperature is subjected to a time-dependent suction. We choose a Cartesian coordinate system where X^*, Y^* -axes are chosen along the plate and normal to the plate, respectively.

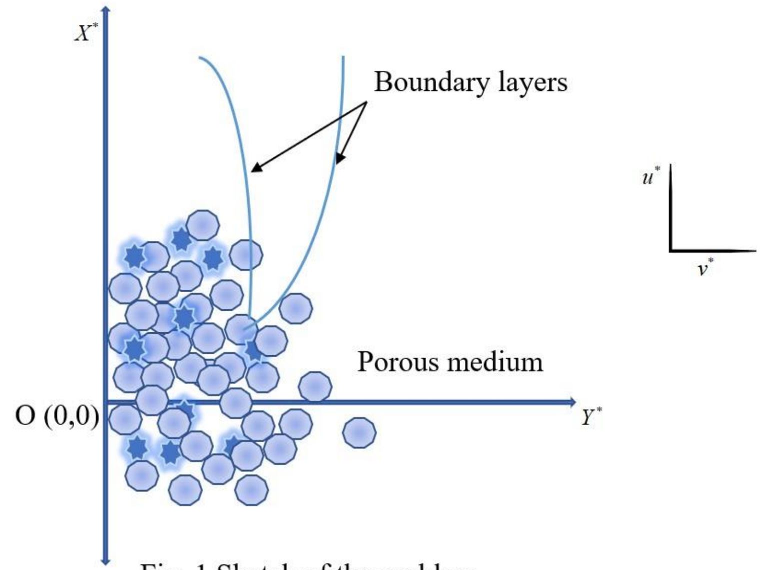

Fig. 1 Sketch of the problem

The governing equations read as follows.

$$\frac{\partial v^*}{\partial y^*}=0 \tag{1}$$

$$\frac{\partial u^*}{\partial t^*}+v^*\frac{\partial u^*}{\partial y^*}=\left(\upsilon+\upsilon_r\right)\frac{\partial^2 u^*}{\partial y^{*2}}+g\beta\left(T-T_\infty\right)-\upsilon\frac{u^*}{K^*}+2\upsilon_r\frac{\partial\omega^*}{\partial y^*}-\frac{1}{\rho}\frac{\partial p^*}{\partial x^*} \tag{2}$$

$$\rho j^*\left(\frac{\partial\omega^*}{\partial t^*}+v^*\frac{\partial\omega^*}{\partial y^*}\right)=\gamma\frac{\partial^2\omega^*}{\partial y^{*2}} \tag{3}$$

$$\frac{\partial T}{\partial t^*}+v^*\frac{\partial T}{\partial y^*}=\frac{\kappa}{\rho c_p}\frac{\partial^2 T}{\partial y^{*2}}+\frac{Q_0}{\rho c_p}\left(T-T_\infty\right) \tag{4}$$

Boundary conditions are

$$\begin{aligned} &y^*=0 \quad ; u^*=u_p^*; T=T_w \ ; \ \omega^*=-N\frac{\partial u^*}{\partial y^*} \\ &y^*\to\infty \ ; u^*\to u_\infty^*=U_0\left(1+\varepsilon e^{\delta^* t^*}\right) \ ; T\to T_\infty \ ; \ \omega^*\to 0 \end{aligned} \tag{5}$$

Where u^*, v^* are velocity components in X^*, Y^* direction respectively, ρ is the fluid density, υ is the kinematic viscosity, υ_r is the kinematic rotational viscosity, β is the coefficient of volumetric thermal expansion of fluid, K^* is the permeability of the porous medium, j^* is the microinertia density, ω^* is the component of angular velocity, γ is the spin gradient viscosity, κ is thermal conductivity, T is temperature, c_p is specific heat at constant pressure, Q_0 is heat sink ,u_p^* velocity of porous plate, U_∞^* is the free stream velocity which follow an exponentially small perturbation law in which ε and δ^* are small less than unity and U_0 is a scale of free stream velocity, T_w the temperature at the wall, T_∞ shows free stream temperature, the boundary condition for microrotation describes it's with the surface stress. In this equation, the parameter N is a number between 0 and 1 that relates the micro relationship gyration vector to the shear stress. Value $N=0$ represents the case when the particle density is sufficiently large, leading to the microelement close to the wall being unable to rotate. Value 0.5 indicates weak concentrations, and at $N=1$, flows are believed to represent turbulent boundary layers (Rees and Bassom [34]).

Outside the boundary layer, the equation (2) gives a pressure gradient in the form.

$$-\frac{1}{\rho}\frac{dp^*}{dx^*}=\frac{dU_\infty^*}{dt^*}+\frac{\upsilon}{K^*}U_\infty^* \tag{6}$$

Now, we introduce non-dimensional quantities as follows.

$$u=\frac{u^*}{U_0},\ v=\frac{v^*}{V_0},\ y=\frac{V_0 y^*}{\upsilon},\ U_\infty=\frac{U_\infty^*}{U_0},\ U_p=\frac{u_p^*}{U_0},\ \omega=\frac{\upsilon}{U_0 V_0}\omega^*,\ t=\frac{t^* V_0^2}{\upsilon},\ \theta=\frac{T-T_\infty}{T_w-T_\infty},\ \delta=\frac{\delta^*\upsilon}{V_0^2},\ Da=\frac{K^* V_0^2}{\upsilon^2},$$

$$j=\frac{V_0^2}{\upsilon^2}j^* \tag{7}$$

and spin gradient viscosity γ, which gives some relationship between the coefficient of viscosity and microinertia, is defined as

$$\gamma=\left(\mu+\frac{1}{2}\mu_r\right)j^*=\mu j^*\left(1+\frac{1}{2}\beta\right) \tag{8}$$

Using the above non-dimensional quantities, the governing equations defined by equations (1) - (4) are converted into the following non-dimensional form.

The equation of continuity (1) gives

$$v=-V_0$$

Equations (2) to (4) gives us

$$\frac{\partial u}{\partial t}-\frac{\partial u}{\partial y}=\frac{dU_\infty}{dt}+\frac{1}{Da}\left(U_\infty-u\right)+\left(1+\beta\right)\frac{\partial^2 u}{\partial y^2}+Gr\theta+2\beta\frac{\partial\omega}{\partial y} \tag{9}$$

$$\frac{\partial\omega}{\partial t}-\frac{\partial\omega}{\partial y}=\frac{1}{m_v}\frac{\partial^2\omega}{\partial y^2} \tag{10}$$

$$\frac{\partial\theta}{\partial t}-\frac{\partial\theta}{\partial y}=\frac{1}{Pr}\frac{\partial^2\theta}{\partial y^2}+S\theta \qquad (11)$$

Where $\beta=\frac{\upsilon_r}{\upsilon}=\frac{\mu_r}{\mu}$ stands for viscosity ratio, $Gr=\frac{g\beta\upsilon(T_w-T_\infty)}{U_0V_0^2}$ stands for grashoff number, $m_v=\frac{\rho j\upsilon^3}{\gamma V_0^2}$ stands for parameter related to microrotation vector, $Pr=\frac{\mu c_p}{\kappa}$ stands for Prandtl number, and $S=\frac{\upsilon Q_0}{\rho c_p V_0^2}$ stands for sink parameter.

and boundary conditions given by equation (5)into non-dimensional form is

$$\begin{aligned} &y=0\,;\,u=U_p\,;\,\omega=-N\frac{\partial u}{\partial y}\,;\,\theta=1\\ &y\to\infty\,;\,u\to U_\infty=1+\varepsilon e^{\delta t}\,;\,\omega\to 0\,;\,\theta\to 0\end{aligned} \qquad (12)$$

Entropy generation

The local volumetric rate of entropy generation S_G is given as follows.

$$S_G=\frac{\kappa}{T_\infty^2}\left(\frac{\partial T}{\partial y^*}\right)^2+\frac{\upsilon(1+\beta)}{T_\infty}\left(\frac{\partial u^*}{\partial y^*}\right)^2+\frac{\upsilon}{T_\infty}\frac{u^{*2}}{K^*}+\frac{\gamma\upsilon^2}{\rho j^*T_\infty V_0^2}\left(\frac{\partial\omega^*}{\partial y^*}\right)^2 \qquad (13)$$

The first term in the equation (13) is the irreversibility due to heat transfer, and the second term is the entropy generation due to viscous dissipation.

In non-dimensional form, the entropy generation N_s is obtained as follows.

$$N_S=\frac{S_G}{S_{G_0}}=\left(\frac{\partial\theta}{\partial y}\right)^2+Br\Omega\left[(1+\beta)\left(\frac{\partial u}{\partial y}\right)^2+\frac{1}{Da}u^2+\frac{1}{m_v}\left(\frac{\partial\omega}{\partial y}\right)^2\right] \qquad (14)$$

Where $S_{G_0}=\frac{\kappa V_0^2}{T_\infty^2\upsilon^2}(T_w-T_\infty)^2$ is characteristic entropy, $\Omega=\frac{T_\infty}{T_w-T_\infty}$ is characteristic temperature and $Br=\frac{\upsilon U_0^2}{\kappa(T_w-T_\infty)}$ is Brinkmann number.

Let $N_1=\left(\frac{\partial\theta}{\partial y}\right)^2$ and $N_2=Br\Omega\left[(1+\beta)\left(\frac{\partial u}{\partial y}\right)^2+\frac{1}{Da}u^2+\frac{1}{m_v}\left(\frac{\partial\omega}{\partial y}\right)^2\right]$, then Bejan Number Be is given as

$$Be=\frac{N_1}{N_1+N_2} \qquad (14)$$

Skin friction, couple stress and Nusselt number

We calculate physical quantities of interest, i.e., skin friction coefficient C_f, couple stress coefficient C_m, and Nusselt number Nu, which are expressed as follows

$$C_f=\left.\frac{2\tau_w}{\rho U_0V_0}\right|_{y^*=0},\; C_m=\frac{M_w}{\mu jU_0},\text{ and } Nu=\frac{x\left.\left(\partial T/\partial y^*\right)\right|_{y^*=0}}{T_w-T_\infty} \qquad (15)$$

$$\text{Where, }\tau_w=(\mu+\mu_r)\left.\frac{\partial u^*}{\partial y^*}\right|_{y^*=0}+\mu_r\left.\omega^*\right|_{y^*=0},\text{ and } M_w=\gamma\left.\frac{\partial\omega^*}{\partial y^*}\right|_{y^*=0} \qquad (16)$$

Using equations (7) and (16) the expression in equation (15) provides Skin friction coefficient, Couple stress coefficient and Nusselt number as.

$$C_f = 2\left(1+(1-N)\beta\right)u'(0),\; C_m = \left(1+\frac{1}{2}\beta\right)\omega'(0),\ \text{and}\ N_u/\mathrm{Re} = -\theta'(0) \tag{17}$$

Where $Re = \frac{xV_0}{\upsilon}$ is Reynolds Number

Numerical technique

The unsteady, nonlinear, coupled partial differential equations (9)-(11) with boundary conditions (12) are solved by employing an implicit finite difference scheme of crank-Nicolson type.

The finite difference equations for the setup are as follows.

$$\frac{u_j^{i+1}-u_j^i}{\Delta t} - \frac{u_{j+1}^{i+1}-u_{j-1}^{i+1}+u_{j+1}^i-u_{j-1}^i}{4\Delta y} = \varepsilon\delta e^{\delta i} + \frac{1}{Da}\left(1+\varepsilon e^{\delta i}-u\right)+$$
$$(1+\beta)\left(\frac{u_{j+1}^{i+1}-2u_j^{i+1}+u_{j-1}^{i+1}+u_{j+1}^i-2u_j^i+u_{j-1}^i}{2(\Delta y)^2}\right)+Gr\left(\frac{\theta_j^{i+1}+\theta_j^i}{2}\right)+2\beta\left(\frac{\omega_{j+1}^{i+1}-\omega_{j-1}^{i+1}+\omega_{j+1}^i-\omega_{j-1}^i}{4\Delta y}\right) \tag{18}$$

$$\frac{\omega_j^{i+1}-\omega_j^i}{\Delta t} - \frac{\omega_{j+1}^{i+1}-\omega_{j-1}^{i+1}+\omega_{j+1}^i-\omega_{j-1}^i}{4\Delta y} = \frac{1}{m_v}\left(\frac{\omega_{j+1}^{i+1}-2\omega_j^{i+1}+\omega_{j-1}^{i+1}+\omega_{j+1}^i-2\omega_j^i+\omega_{j-1}^i}{2(\Delta y)^2}\right) \tag{19}$$

$$\frac{\theta_j^{i+1}-\theta_j^i}{\Delta t} - \frac{\theta_{j+1}^{i+1}-\theta_{j-1}^{i+1}+\theta_{j+1}^i-\theta_{j-1}^i}{4\Delta y} = \frac{1}{Pr}\left(\frac{\theta_{j+1}^{i+1}-2\theta_j^{i+1}+\theta_{j-1}^{i+1}+\theta_{j+1}^i-2\theta_j^i+\theta_{j-1}^i}{2(\Delta y)^2}\right)+S\left(\frac{\theta_j^{i+1}+\theta_j^i}{2}\right) \tag{20}$$

and the boundary conditions given in equation (12) are discretized as follows

$$\begin{aligned} &u_j^1 = U_p;\ \omega_j^1 = -N\left(\frac{u_2-u_1}{\Delta y}\right);\ \theta_j^1 = 1 \\ &u_J^n = U_\infty;\ \omega_J^n = 0;\ \theta_J^n = 0 \end{aligned} \tag{21}$$

Here, subscript j denotes the grid point with y -coordinate $j\Delta y$

The above equations can be rewritten as follows

$$a_3u_{j+1}^{i+1}+a_6\omega_{j+1}^{i+1}+a_1u_j^{i+1}+a_5\theta_j^{i+1}+a_4u_{j-1}^{i+1}-a_6\omega_{j-1}^{i+1} = R_{1,j}^i \tag{22}$$

$$b_3\omega_{j+1}^{i+1}+b_1\omega_j^{i+1}+b_4\omega_{j-1}^{i+1} = R_{2,j}^i \tag{23}$$

$$c_3\theta_{j+1}^{i+1}+c_1\theta_j^{i+1}+c_4\theta_{j-1}^{i+1} = R_{3,j}^i \tag{24}$$

Where $R_{1,j}^i = -a_2u_j^i - a_3u_{j+1}^i - a_4u_{j-1}^i - a_6\left(\omega_{j+1}^i-\omega_{j-1}^i\right) - a_5\theta_j^i + \left(\varepsilon\delta+\frac{\varepsilon}{Da}\right)e^{\delta i}+\frac{1}{Da}$,

$R_{2,j}^i = -b_2\omega_j^i - b_3\omega_{j+1}^i - b_4\omega_{j-1}^i$, $R_{3,j}^i = -c_2\theta_j^i - c_3\theta_{j+1}^i - c_4\theta_{j-1}^i$,

$$a_1=\frac{1}{\Delta t}+\frac{1}{2Da}+\frac{1+\beta}{(\Delta y)^2},\quad a_2=-\frac{1}{\Delta t}+\frac{1}{2Da}+\frac{1+\beta}{(\Delta y)^2},\quad a_3=-\frac{1}{4\Delta y}-\frac{1+\beta}{2(\Delta y)^2},\quad a_4=\frac{1}{4\Delta y}-\frac{1+\beta}{2(\Delta y)^2},\quad a_5=-\frac{Gr}{2},$$

$$a_6=-\frac{\beta}{2\Delta y},\quad b_1=\frac{1}{\Delta t}+\frac{1}{m_v(\Delta y)^2},\quad b_2=-\frac{1}{\Delta t}+\frac{1}{m_v(\Delta y)^2},\quad b_3=-\frac{1}{4\Delta y}-\frac{1}{2m_v(\Delta y)^2},\quad b_4=\frac{1}{4\Delta y}-\frac{1}{2m_v(\Delta y)^2},$$

$$c_1=\frac{1}{\Delta t}+\frac{1}{Pr(\Delta y)^2}-\frac{S}{2},\ c_2=-\frac{1}{\Delta t}+\frac{1}{Pr(\Delta y)^2}-\frac{S}{2},\ c_3=-\frac{1}{4\Delta y}-\frac{1}{2Pr(\Delta y)^2},\ \text{and}\ c_4=\frac{1}{4\Delta y}-\frac{1}{2Pr(\Delta y)^2}$$

We notice that the finite difference equations (18)-(20) for each time step have a block tri-diagonal matrix that is amenable to Thomas algorithm treatment.

In vector-matrix notation, equations (22)-(24) can be written as

AX=C

$$A=\begin{bmatrix} D_1 & A_1 & & & & \\ B_2 & D_2 & A_2 & & & \\ & B_3 & D_3 & A_3 & & \\ & & \ddots & \ddots & \ddots & \\ & & & B_{m-1} & D_{m-1} & A_{m-1} \\ & & & & B_m & D_m \end{bmatrix},\ X=\begin{bmatrix} X_1 \\ X_2 \\ X_3 \\ \vdots \\ X_{m-1} \\ X_m \end{bmatrix},\ C=\begin{bmatrix} C_1 \\ C_2 \\ C_3 \\ \vdots \\ C_{m-1} \\ C_m \end{bmatrix}$$

Where, $X_j=\begin{bmatrix} u_j & \omega_j & \theta_j \end{bmatrix},\ 1\le j\le J$, $D_1=\begin{bmatrix} 1 & 0 & 0 \\ -N/k & 1 & 0 \\ 0 & 0 & 1 \end{bmatrix}$, $A_1=\begin{bmatrix} 0 & 0 & 0 \\ N/k & 0 & 0 \\ 0 & 0 & 0 \end{bmatrix}$, $C_1=\begin{bmatrix} U_p & 0 & 1 \end{bmatrix}^T$.

$$D_j=\begin{bmatrix} a_1 & 0 & a_5 \\ 0 & b_1 & 0 \\ 0 & 0 & c_1 \end{bmatrix},2\le j\le J-1,\quad A_j=\begin{bmatrix} a_3 & a_6 & 0 \\ 0 & b_3 & 0 \\ 0 & 0 & c_3 \end{bmatrix},2\le j\le J-1,\quad B_j=\begin{bmatrix} a_4 & -a_6 & 0 \\ 0 & b_4 & 0 \\ 0 & 0 & c_4 \end{bmatrix},2\le j\le J-1,$$

$$B_J=\begin{bmatrix} 0 & 0 & 0 \\ 0 & 0 & 0 \\ 0 & 0 & 0 \end{bmatrix},\ D_J=\begin{bmatrix} 1 & 0 & 0 \\ 0 & 1 & 0 \\ 0 & 0 & 1 \end{bmatrix},\ C_J=\begin{bmatrix} 1+\varepsilon e^{\delta t} & 0 & 0 \end{bmatrix}^T,\ C_j=\begin{bmatrix} R_{1,j} & R_{2,j} & R_{3,j} \end{bmatrix},2\le j\le J-1$$

The computations carried through the above scheme provide quantities of interest, viz. Values of skin friction coefficient C_f, couple stress coefficient C_m, Nusselt number Nu, velocity and temperature profiles. These quantities are instrumental in computing thermodynamic irreversibility.

Table 1: Values of Skin Friction Coefficient C_f, couple Stress coefficient C_m, and Nusselt number Nu for various values of Da, β, Gr, m_v, U_p, and N with $t=0.3,\ Pr=1,\ S=-1,\ \delta=0.01,\ \Omega=1,$ and $Br=5$ at wall $y^*=0$

Da	β	Gr	m_v	U_p	N	C_f	C_m	Nu
0.1	0.5	2	0.5	0.5	0.5	4.894375	8.040208	1.813906
0.2						3.523349	8.040137	
0.3						2.664230	7.914999	
0.5						1.682003	7.697730	
1	0	2	0.5	0.5	0.5	0.645275	5.783535	1.813906
	1					0.741437	9.012886	
	5					1.062313	20.48592	
	10					1.313380	32.93657	
1	0.5	1	0.5	0.5	0.5	0.119091	7.229373	1.813906
		3				1.265227	7.616370	

		5				2.411363	8.003367	
		7				3.557498	8.390364	
1	0.5	2	0.3	0.5	0.5	0.683140	7.749395	1.813906
			0.5			0.692159	7.422872	
			0.7			0.698834	6.951494	
			0.9			0.704068	6.512866	
1	0.5	2	0.5	0.1	0.5	2.377509	2.235170	1.813906
				0.5		0.692159	7.422872	
				2		-5.62790	26.87675	
				3		-9.84127	39.84600	
1	0.5	2	0.5	0.5	0.1	0.747741	1.541506	1.813906
					0.4	0.706051	5.996713	
					0.7	0.664158	10.18435	
					1	0.620659	14.10310	

Table 2: Values of Skin Friction Coefficient C_f, couple Stress coefficient C_m, and Nusselt number Nu for various values of Pr, S with $t=0.3$, $Da=1$, $\beta=0.5$, $Gr=2$, $m_v=0.5$, $U_p=0.5$, $N=0.5$, $\delta=0.01$, $\Omega=1$, $Br=5$ at wall $y^*=0$

Pr	S	C_f	C_m	Nu
1	-1	0.692159	7.422872	1.813906
3		0.220738	7.254799	4.069821
5		0.039607	7.191697	6.032739
7		-0.062975	7.156649	7.902097
1	-1	0.692159	7.422872	1.813906
	-5	0.511831	7.342274	2.724067
	-10	0.367424	7.283858	3.570906
	-15	0.271525	7.248312	4.241679

Result and discussion

To peep into the phenomenon of thermodynamic irreversibility confronted by the system, the plots for entropy number Ns and Bejan number have been depicted in 2-D and 3-D setups. Besides these, the plots for velocity, temperature and microrotation have been appended in the appendix to have a ready glance, as these also impact entropy generation. We recall the entropy number is composed of two parts, viz., the heat transfer part and the dissipative part, which involve parameters having a bearing on the system. Consequently, a parametric study of thermodynamic irreversibility is possible. The Bejan number is another parameter that identifies relative contribution. Besides the plots, we showcase pertinent quantities, viz. skin friction coefficient C_f, couple stress coefficient C_m and Nusselt number Nu in Tables 1 and 2.

From the table-1, we notice that with the increasing value of Darcy number Da from 0.1 to 0.5, the coefficient of skin friction is decreased from 4.894375 to 1.682003, and couple stress gets decreased from 8.040208 to 7.697730, and Nusselt number remains unchanged while the other parameters are kept fixed as $\beta=0.5$, $Gr=2$, $m_v=0.5$, $Pr=1$, $S=-1$, $U_p=0.5$, $N=0.5$, $\delta=0.01$, $\Omega=1$, and $Br=5$. With the increasing value of viscosity ratio β from 0 to 10 the coefficient of skin friction got increased from 0.645275 to 1.313380 and coefficient of couple stress increased from 5.783535 to 32.936571 while the parameters are kept fixed as $Da=1$, $Gr=2$, $m_v=0.5$, $Pr=1$, $S=-1$, $U_p=0.5$, $N=0.5$, $\delta=0.01$, $\Omega=1$, and $Br=5$. With the increasing value of Grashoff number Gr from 1 to 7 the coefficient of skin friction increased from 0.119091 to 3.557498 and coefficient of couple stress increased from 7.229373 to 8.390364 when parameters are kept fixed as $Da=1, \beta=0.5$, $m_v=0.5$, $Pr=1$, $S=-1$, $U_p=0.5$, $N=0.5$, $\delta=0.01$, $\Omega=1$, and $Br=5$. With the increasing value of m_v (parameter related to microrotation) from 0.3 to 0.9, the coefficient of skin friction increased from 0.683140 to 0.704068, and the coefficient of couple stress decreased from 7.749395 to 6.512866 when parameters were kept fixed as $Da=1, \beta=0.5$, $Gr=2$, $Pr=1$, $S=-1$, $U_p=0.5$, $N=0.5$, $\delta=0.01$, $\Omega=1$, and $Br=5$. With the increasing value of the velocity U_p at the wall $y^*=0$ from 0.1 to 3, the coefficient of skin friction decreased from 2.377509 to -9.841279, and the coefficient of couple stress jumped from 2.235170 to 39.846007 when parameters are kept fixed as $Da=1, \beta=0.5$, $Gr=2$, $m_v=0.5$, $Pr=1$, $S=-1$, $N=0.5$, $\delta=0.01$, $\Omega=1$, and $Br=5$. With the increasing value of N (parameter relates micro gyration to the shear stress) from 0.1 to 1, the coefficient of skin friction decreased from 0.747741709048447 to 0.620659017053793, and the coefficient of couple stress increased from 1.541506 to 14.103106. In contrast, the parameters are kept fixed as $Da=1, \beta=0.5$, $Gr=2$, $m_v=0.5$, $Pr=1$, $S=-1$, $U_p=0.5$, $\delta=0.01$, $\Omega=1$, and $Br=5$.

Table 2 data shows that with increasing value of Prandtl number Pr from 1 to 7, the coefficient of skin friction decreased from 0.692159 to -0.062971, the coefficient of couple stress decreased from 7.422872 to 7.156649, and the Nusselt number increased from 1.813906 to7.90209751920219. At the same time, parameters are kept fixed as $Da=1, \beta=0.5$, $Gr=2$, $m_v=0.5$, $S=-1$, $U_p=0.5$, $N=0.5$, $\delta=0.01$, $\Omega=1$, and $Br=5$. When the sink parameter S is changed from -1 to -15 then the coefficient of skin friction decreased from 0.692159 to 0.271525, coefficient of couple stress decreased from 7.422872 to 7.248312, and Nusselt Number registered a jump from 1.813906 to 4.241679 while parameters are kept fixed as $Da=1$, $\beta=0.5$, $Gr=2$, $m_v=0.5$, $Pr=1$, $U_p=0.5$, $N=0.5$, $\delta=0.01$, $\Omega=1$, and $Br=5$

To peep into the phenomenon of thermodynamic irreversibility confronted by the system, the plots for entropy number Ns and Bejan number Be have been depicted in 2-D and 3-D setups. Besides these, the plots for velocity, temperature and microrotation have been appended in the appendix to have a ready glance, as these also impact entropy generation. We recall the entropy number is composed of two parts viz. The heat transfer part and the dissipative part involve parameters having a bearing on the system. Consequently, a parametric study of thermodynamic irreversibility is possible. Besides the plots, we showcase pertinent quantities. From these figures, we notice the dependence of entropy on embedded parameters, indicating that entropy can be managed qualitatively and quantitatively by proper selection of parameters paving the way for entropy generation minimization.

The present study aimed solely to fill the void of solution strategy for such setups hitherto attempted by perturbation methods. Our endeavour offers an outreach to robust numerical treatment.

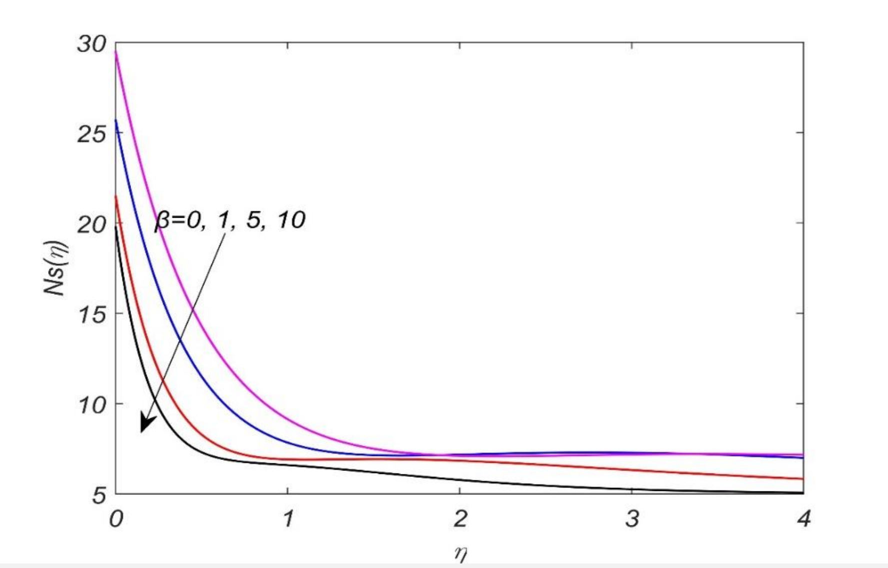

Figure 2: Entropy with varying β **when** $Da=1$, $Gr=2$, $m_v=0.5$, $Pr=1$, $S=-1$, $U_p=0.5$, $N=0.5$, $\delta=0.01$, $\Omega=1$, **and** $Br=5$.

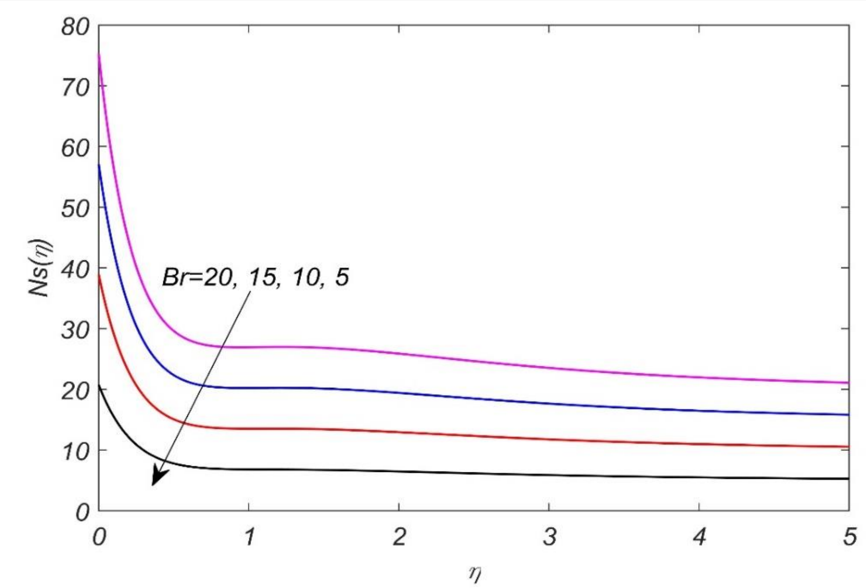

Figure 3: Entropy generation profile for varying Br **when** $\beta=0.5$, $Da=1$, $Gr=2$, $m_v=0.5$, $Pr=1$, $S=-1$, $U_p=0.5$, $N=0.5$, $\delta=0.01$, **and** $\Omega=1$.

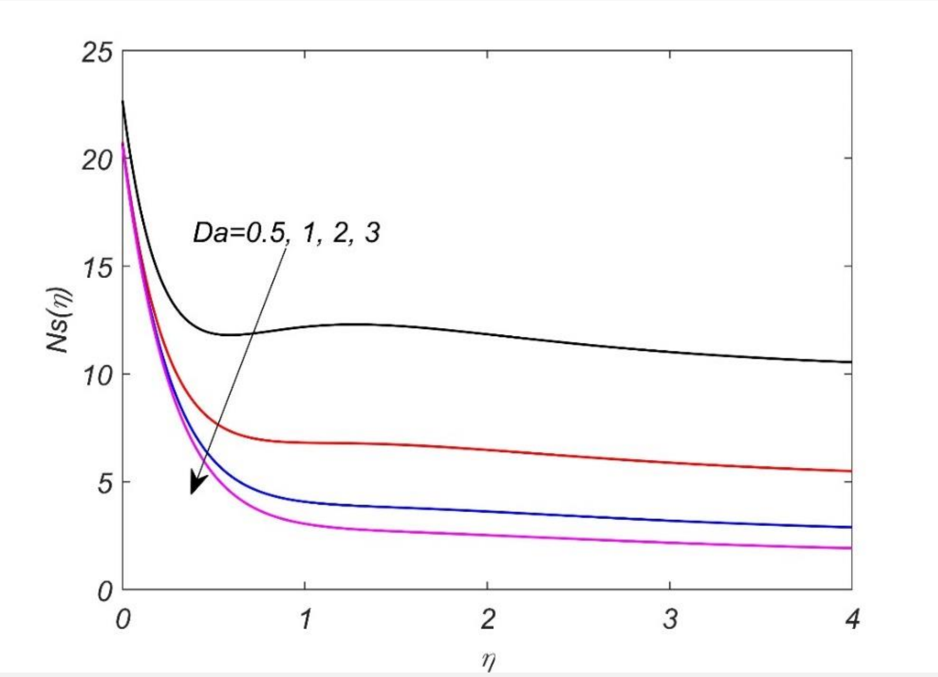

Figure 4: Entropy generation profile for varying Da **when** $\beta = 0.5$, $Gr = 2$, $m_v = 0.5$, $Pr = 1$, $S = -1$, $U_p = 0.5$, $N = 0.5$, $\delta = 0.01$, $\Omega = 1$, **and** $Br = 5$.

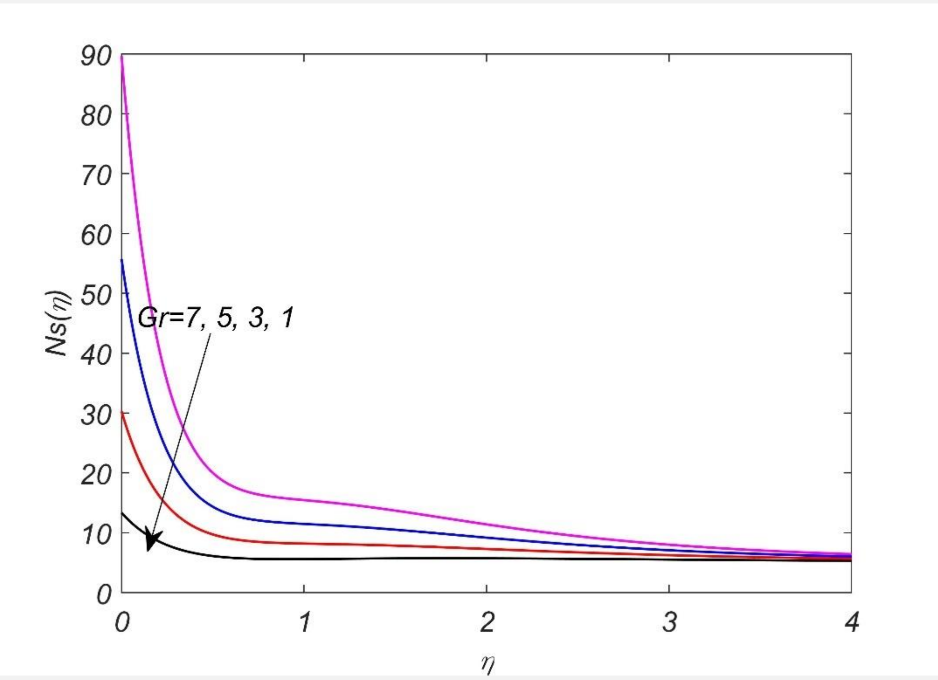

Figure 5: Entropy generation profile for varying Gr **when** $\beta = 0.5$, $Da = 1$, $m_v = 0.5$, $Pr = 1$, $S = -1$, $U_p = 0.5$, $N = 0.5$, $\delta = 0.01$, $\Omega = 1$, **and** $Br = 5$.

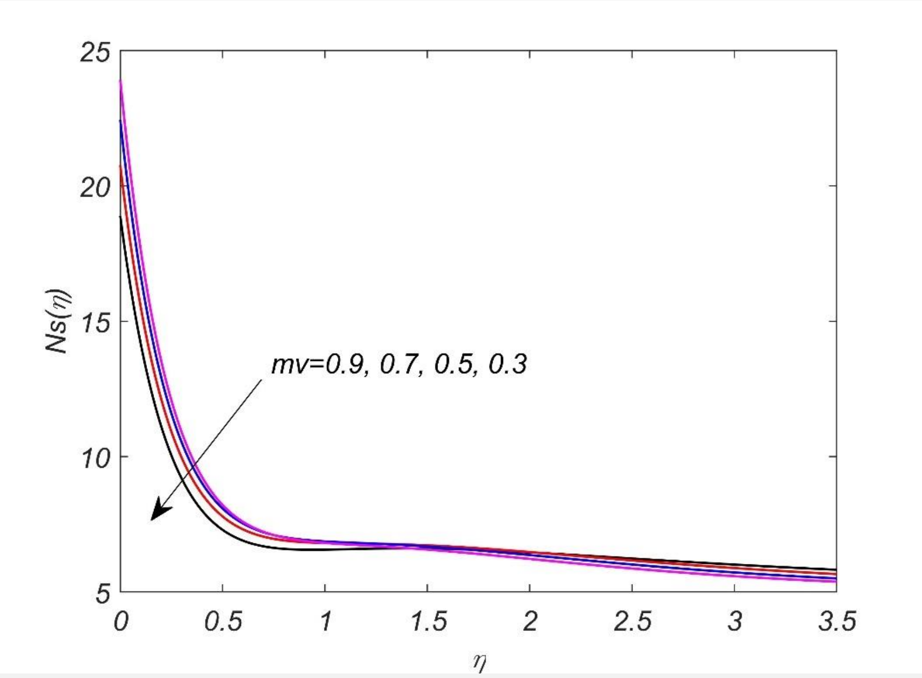

Figure 6: Entropy generation profile for varying m_v **when** $\beta = 0.5$, $Da = 1$, $Gr = 2$, $Pr = 1$, $S = -1$, $U_p = 0.5$, $N = 0.5$, $\delta = 0.01$, $\Omega = 1$, **and** $Br = 5$.

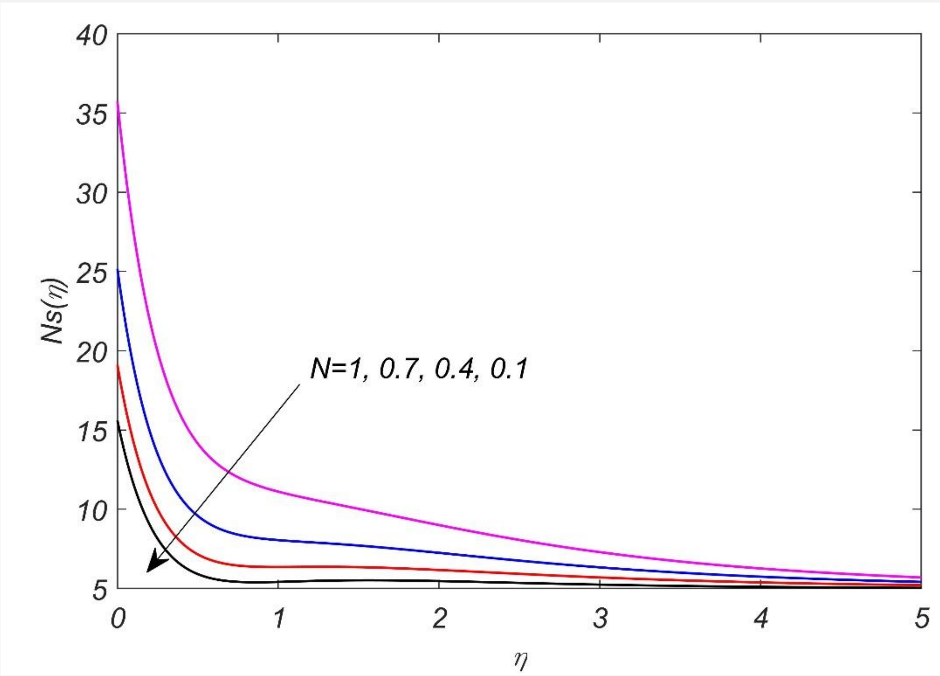

Figure 7: Entropy generation profile for varying N **when** $\beta = 0.5$, $Da = 1$, $Gr = 2$, $m_v = 0.5$, $Pr = 1$, $S = -1$, $U_p = 0.5$, $\delta = 0.01$, $\Omega = 1$, **and** $Br = 5$.

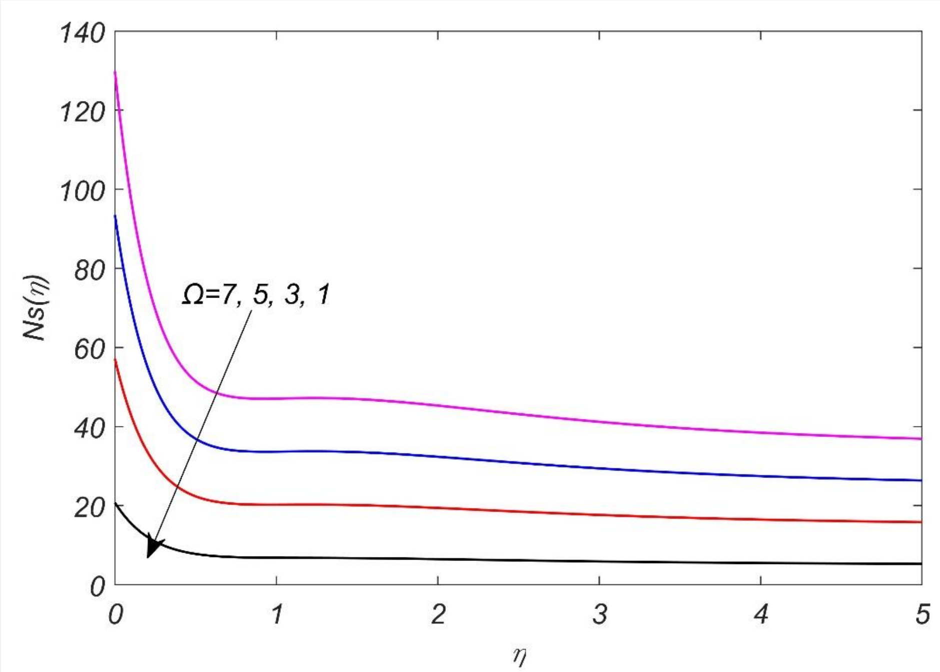

Figure 8: Entropy generation profile for varying Ω **when** $\beta = 0.5$, $Da = 1$, $Gr = 2$, $m_v = 0.5$, $Pr = 1$, $S = -1$, $U_p = 0.5$, $N = 0.5$, $\delta = 0.01$, **and** $Br = 5$.

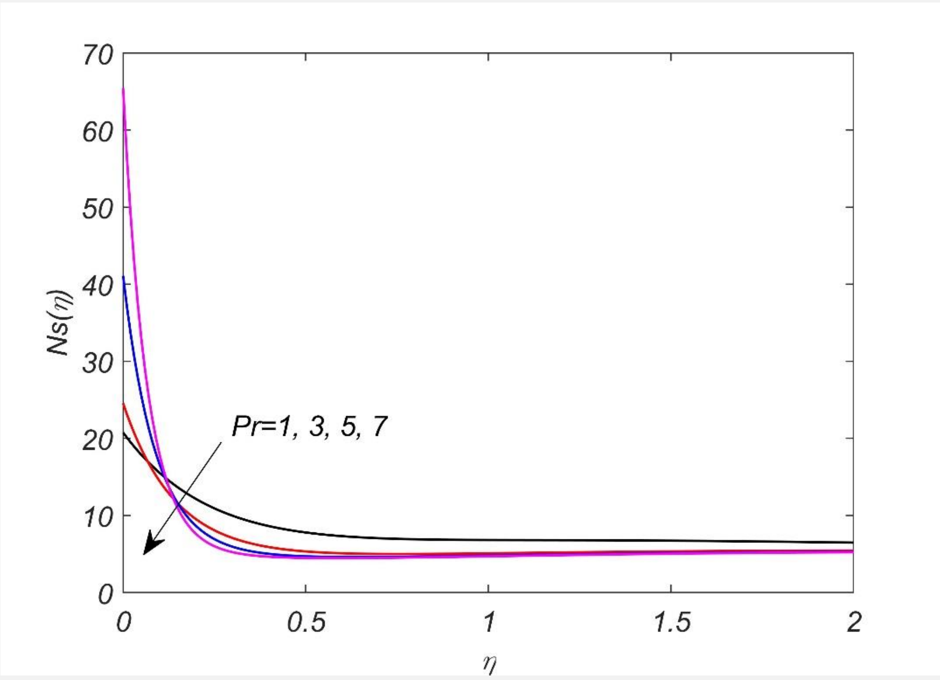

Figure 9: Entropy generation profile for varying $\Pr$ **when** $\beta = 0.5$, $Da = 1$, $Gr = 2$, $m_v = 0.5$, $S = -1$, $U_p = 0.5$, $N = 0.5$, $\delta = 0.01$, $\Omega = 1$, **and** $Br = 5$.

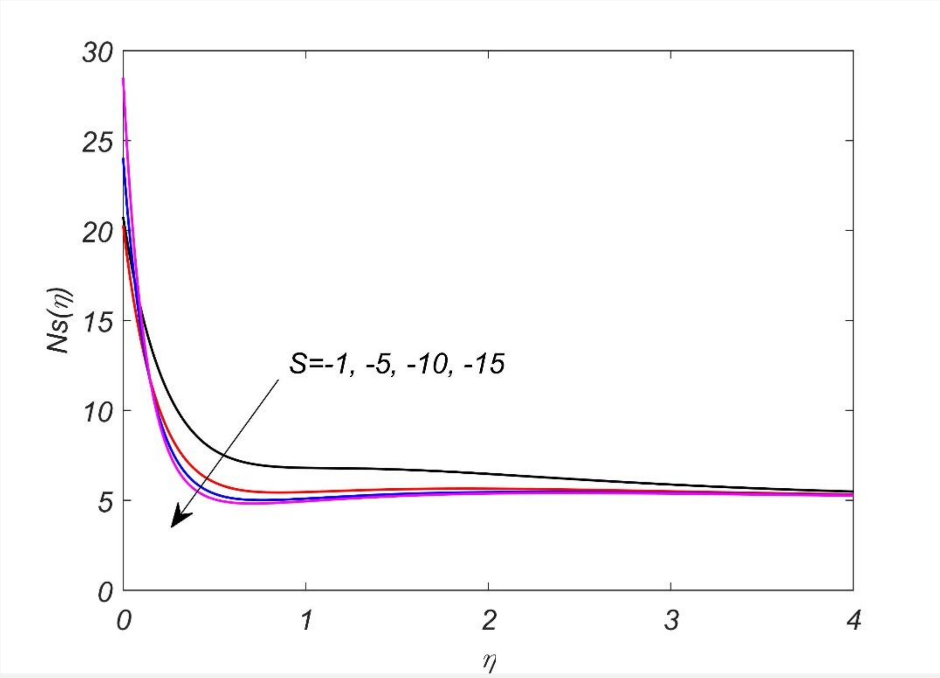

Figure 10: Entropy generation profile for varying S **when** $\beta = 0.5$, $Da = 1$, $Gr = 2$, $m_v = 0.5$, $Pr = 1$, $U_p = 0.5$, $N = 0.5$, $\delta = 0.01$, $\Omega = 1$, **and** $Br = 5$.

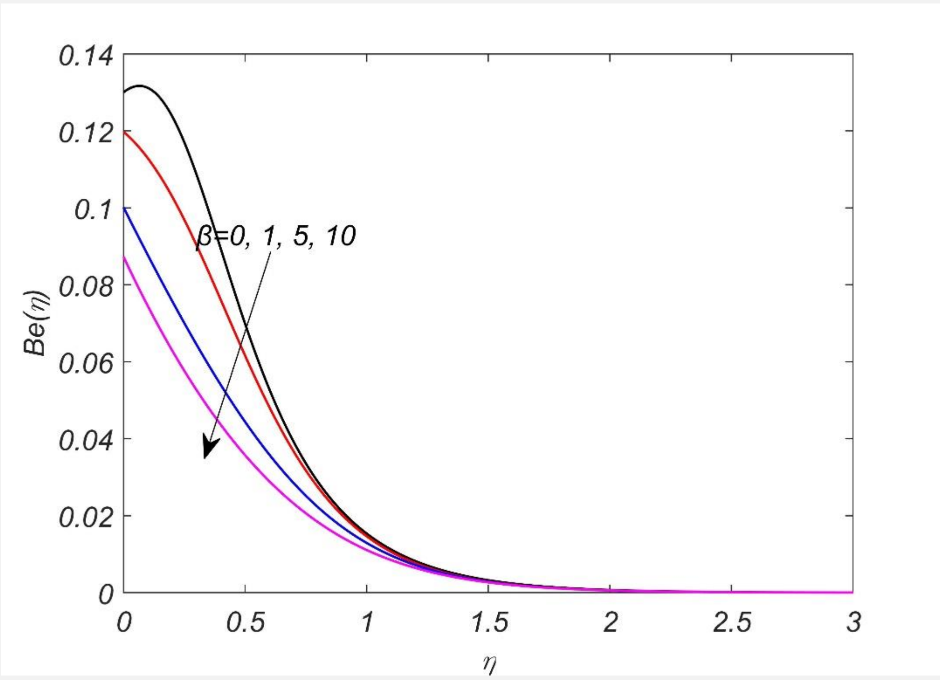

Figure 11: Bejan number profile for varying β **when** $Da = 1$, $Gr = 2$, $m_v = 0.5$, $Pr = 1$, $S = -1$, $U_p = 0.5$, $N = 0.5$, $\delta = 0.01$, $\Omega = 1$, **and** $Br = 5$.

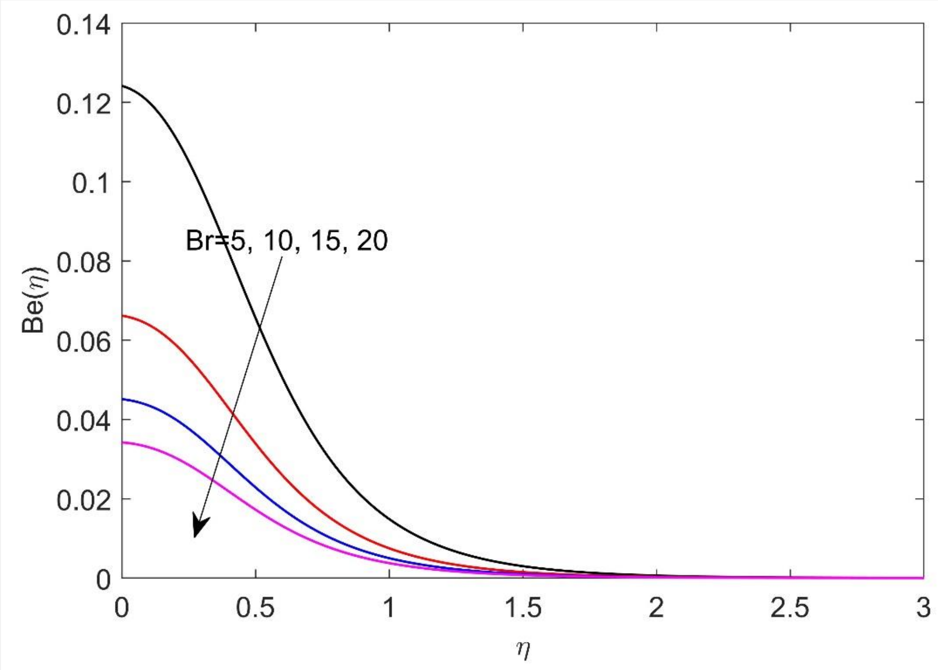

Figure 12: Bejan number profile for varying Br **when** $\beta = 0.5$, $Da = 1$, $Gr = 2$, $m_v = 0.5$, $Pr = 1$, $S = -1$, $U_p = 0.5$, $N = 0.5$, $\delta = 0.01$ **and,** $\Omega = 1$.

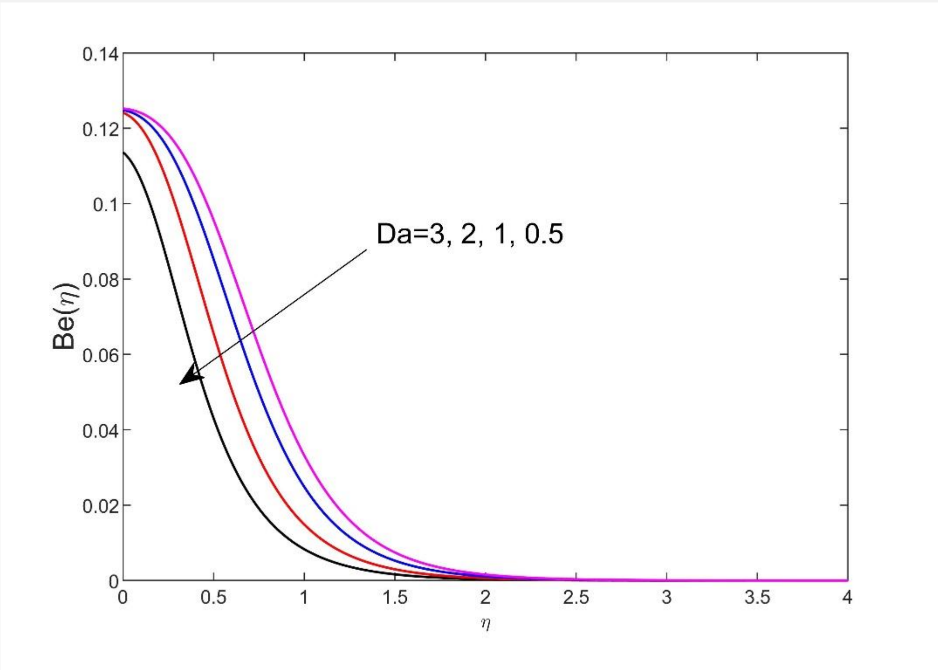

Figure 13: Bejan number profile for varying Da. **when** $\beta = 0.5$, $Gr = 2$, $m_v = 0.5$, $Pr = 1$, $S = -1$, $U_p = 0.5$, $N = 0.5$, $\delta = 0.01$, $\Omega = 1$, **and** $Br = 5$.

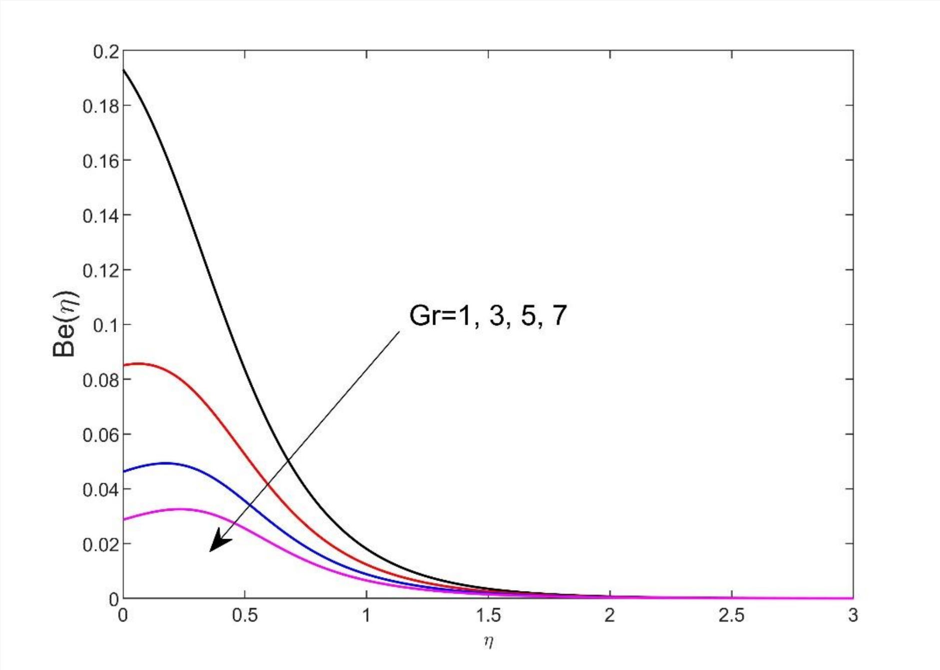

Figure 14: Bejan number profile for varying Gr **when** $\beta = 0.5$, $Da = 1$, $m_v = 0.5$, $Pr = 1$, $S = -1$, $U_p = 0.5$, $N = 0.5$, $\delta = 0.01$, $\Omega = 1$, **and** $Br = 5$.

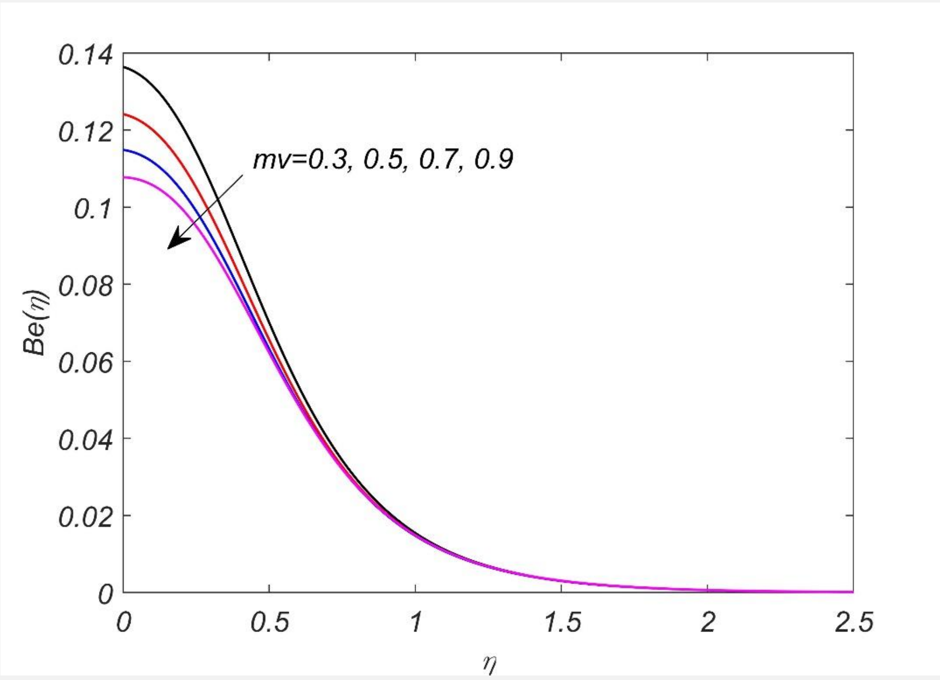

Figure 15: Bejan number profile for varying m_v **when** $\beta = 0.5$, $Da = 1$, $Gr = 2$, $Pr = 1$, $S = -1$, $U_p = 0.5$, $N = 0.5$, $\delta = 0.01$, $\Omega = 1$, **and** $Br = 5$.

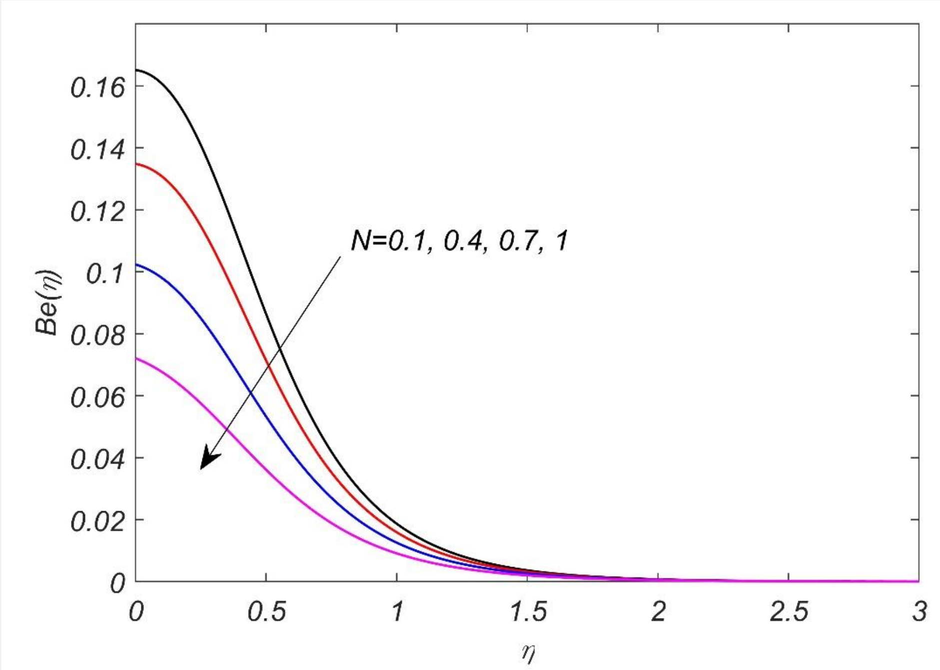

Figure 16: Bejan number profile for varying N **when** $\beta = 0.5$, $Da = 1$, $Gr = 2$, $m_v = 0.5$, $Pr = 1$, $S = -1$, $U_p = 0.5$, $\delta = 0.01$, $\Omega = 1$, **and** $Br = 5$.

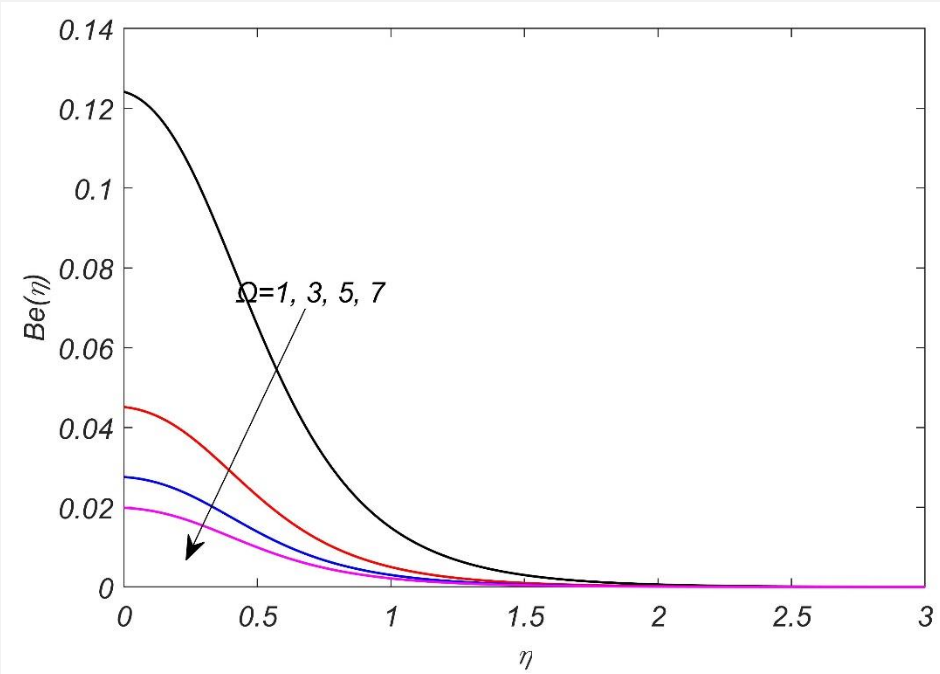

Figure 17: Bejan number profile for varying Ω. **when** $\beta = 0.5$, $Da = 1$, $Gr = 2$, $m_v = 0.5$, $Pr = 1$, $S = -1$, $U_p = 0.5$, $N = 0.5$, $\delta = 0.01$, **and** $Br = 5$.

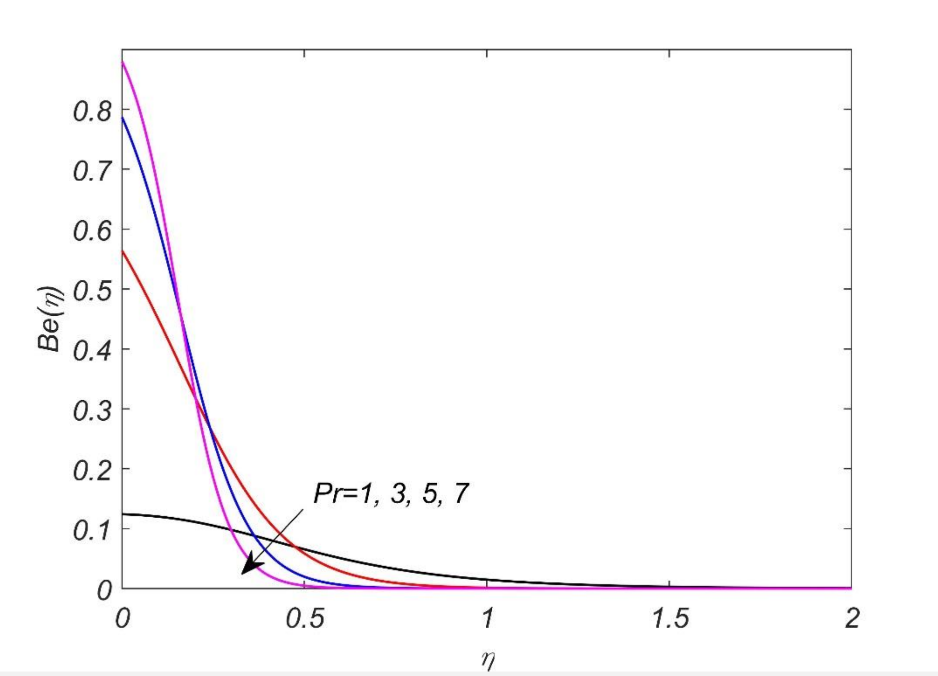

Figure 18: Bejan number profile for varying Pr **when** $\beta = 0.5$, $Da = 1$, $Gr = 2$, $m_v = 0.5$, $S = -1$, $U_p = 0.5$, $N = 0.5$, $\delta = 0.01$, $\Omega = 1$, **and** $Br = 5$.

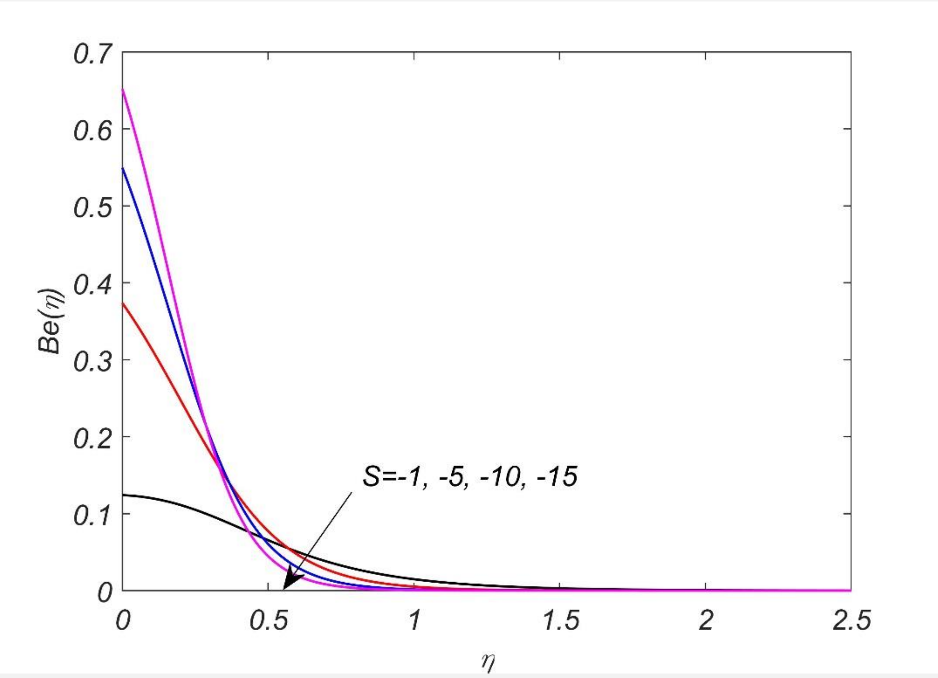

Figure 19: Bejan number profile for varying S when $\beta = 0.5$, $Da = 1$, $Gr = 2$, $m_v = 0.5$, $Pr = 1$, $U_p = 0.5$, $N = 0.5$, $\delta = 0.01$, $\Omega = 1$, **and** $Br = 5$.

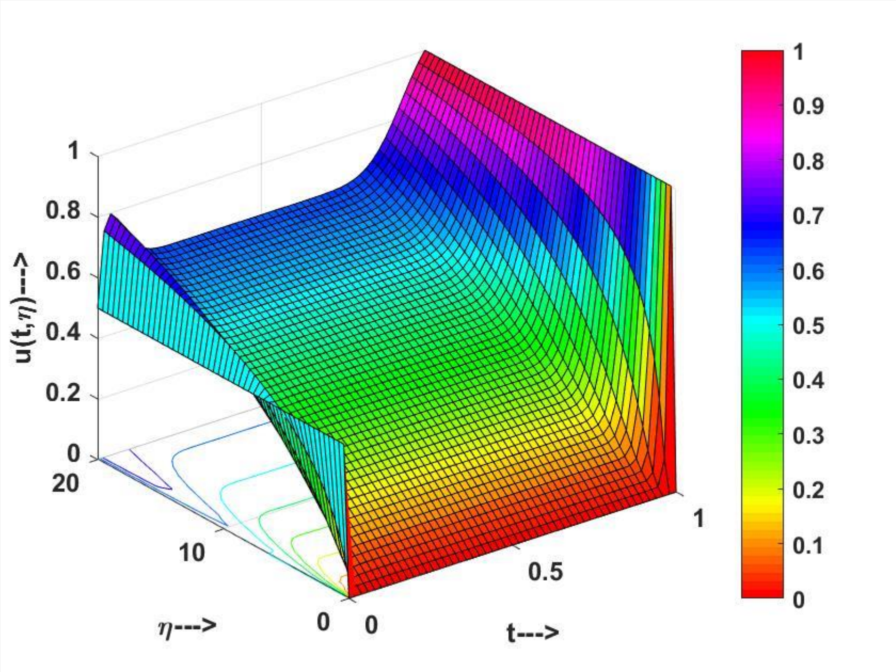

Figure 20: Three Dimensional velocity profile when $\beta = 0.5$, $Da = 1$, $Gr = 2$, $m_v = 0.5$, $Pr = 1$, $U_p = 0.5$, $N = 0.5$, $\delta = 0.01$, $\Omega = 1$, **and** $Br = 5$

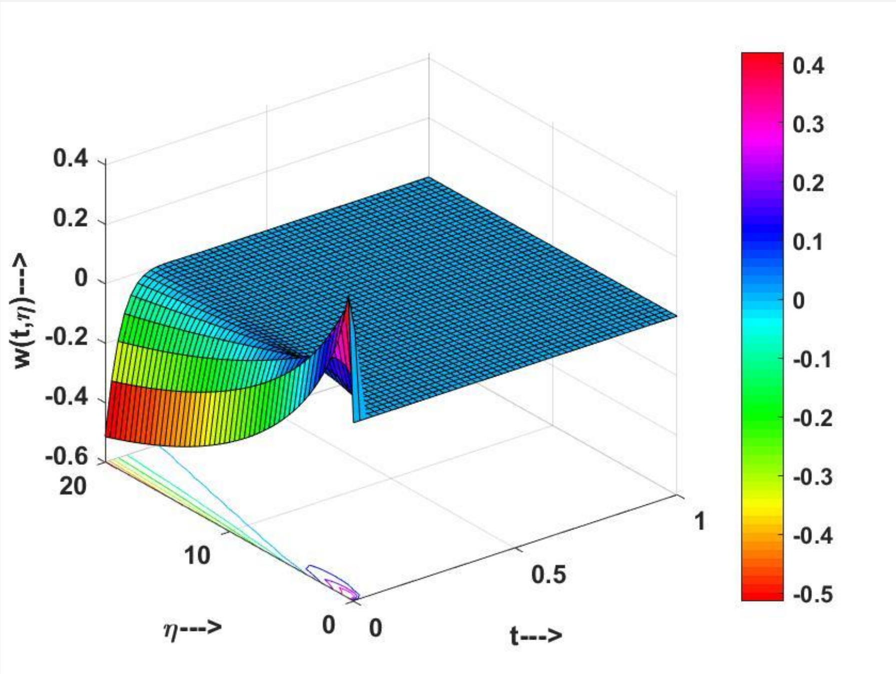

Figure 21: Three Dimensional microrotation profile when $\beta = 0.5$, $Da = 1$, $Gr = 2$, $m_v = 0.5$, $Pr = 1$, $U_p = 0.5$, $N = 0.5$, $\delta = 0.01$, $\Omega = 1$, **and** $Br = 5$

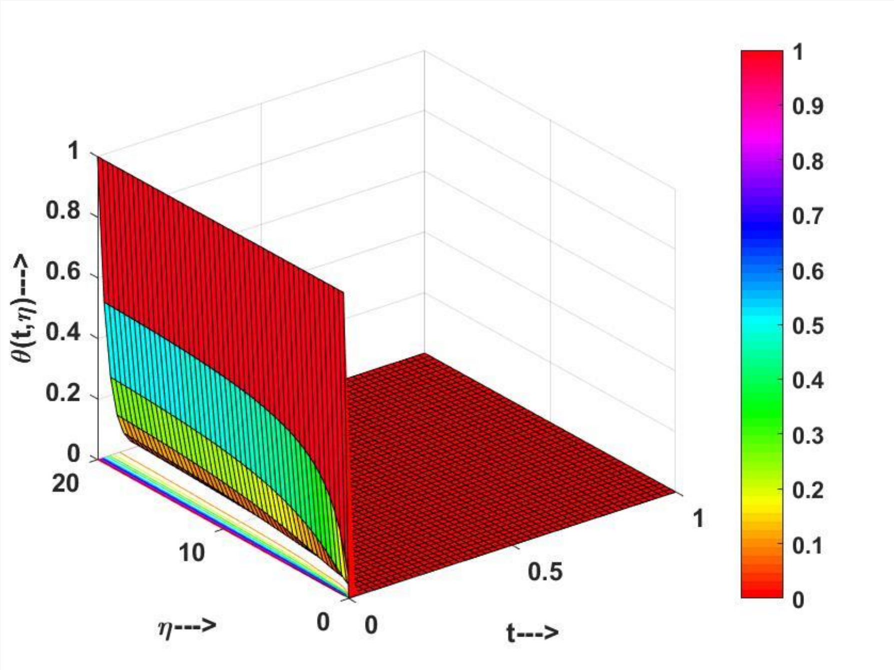

Figure 22: Three Dimensional temperature profile when $\beta = 0.5$, $Da = 1$, $Gr = 2$, $m_v = 0.5$, $Pr = 1$, $U_p = 0.5$, $N = 0.5$, $\delta = 0.01$, $\Omega = 1$, **and** $Br = 5$

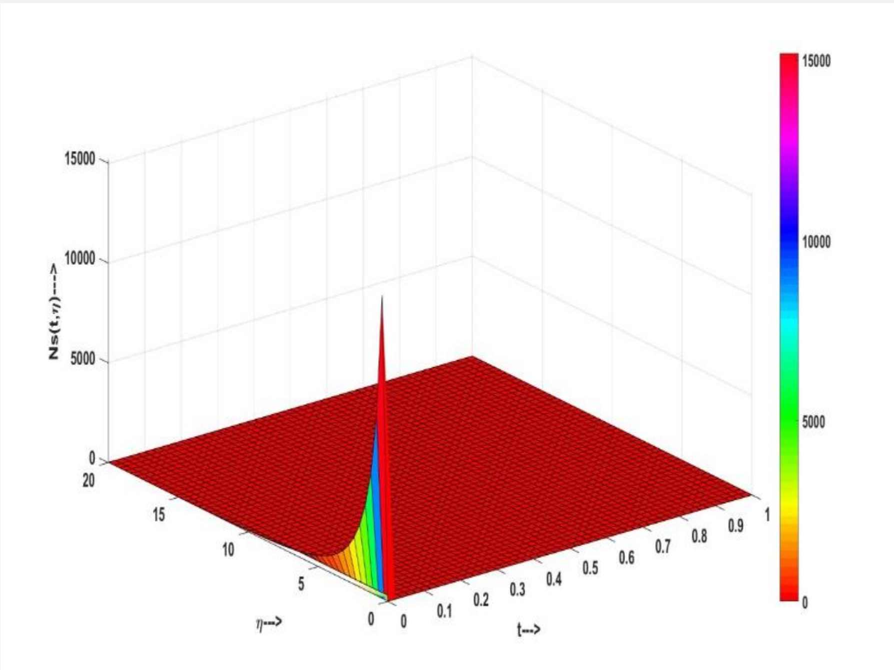

Figure 22: Three Dimensional Entropy generation profile when $\beta = 0.5$, $Da = 1$, $Gr = 2$, $m_v = 0.5$, $Pr = 1$, $U_p = 0.5$, $N = 0.5$, $\delta = 0.01$, $\Omega = 1$, **and** $Br = 5$

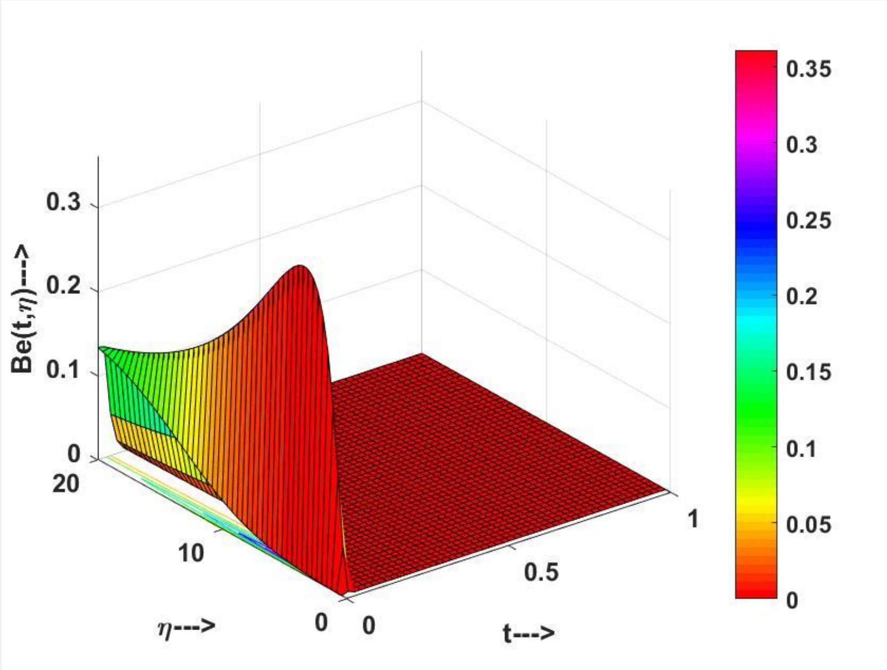

Figure 23: Three Dimensional Bejan Number profile when $\beta = 0.5$, $Da = 1$, $Gr = 2$, $m_v = 0.5$, $Pr = 1$, $U_p = 0.5$, $N = 0.5$, $\delta = 0.01$, $\Omega = 1$, **and** $Br = 5$

References

[1] Bejan A. Second-law analysis in heat transfer and thermal design. Adv heat Transf. 1982;15:352.

[2] Bejan A. Entropy generation minimization: The new thermodynamics of finite-size devices and finite-time processes. J Appl Phys. 1996;79(3):1191-1218. doi:10.1063/1.362674

[3] Rashidi MM, Abelman S, Mehr NF. Entropy generation in steady MHD flow due to a rotating porous disk in a nanofluid. Int J Heat Mass Transf. 2013;62(1):515-525. doi:10.1016/j.ijheatmasstransfer.2013.03.004

[4] Maougal A, Bessaïh R. Heat Transfer and Entropy Analysis for Mixed Convection in a Discretely Heated Porous Square Cavity. Vol 9.; 2013.

[5] Vyas P, Srivastava N. Entropy Analysis of Generalized MHD Couette Flow Inside a Composite Duct with Asymmetric Convective Cooling. Arab J Sci Eng. 2015;40(2):603-614. doi:10.1007/s13369-014-1562-0

[6] Habibi Matin M. Entropy Analysis of Combined Heat and Mass Transfer over a Plate Embedded in a Porous Medium. J Mech Eng Autom. 2015;5(3A):26-32. doi:10.5923/c.jmea.201501.05

[7] Vyas P, Khan S. Entropy Analysis for MHD Dissipative Casson Fluid Flow in Porous Medium Due to Stretching Cylinder 1. Vol 61.; 2016. http://journal.it.cas.cz

[8] Srivastava N, Vyas P, Soni S. Entropy generation analysis for oscillatory flow in a vertical channel filled with porous medium. In: 2016 International Conference on Recent Advances and Innovations in Engineering, ICRAIE 2016. Vol 0. ; 2017:0-5. doi:10.1109/ICRAIE.2016.7939542

[9] Vyas P, Soni S. Entropy analysis for boundary layer flow due to a point sink at the vertex of the cone. Acta Tech CSAV (Ceskoslovensk Akad Ved). 2018;63(2):143-156.

[10] Samantha Kumari S, Sankara Sekhar Raju G. Unsteady MHD free convective flow past a vertical porous plate with span-wise fluctuating heat and mass transfer effects. Fluid Dyn Mater Process. 2019;15(5):471-189. doi:10.32604/fdmp.2019.04222

[11] Vyas P, Kasana RK, Khan S. Entropy analysis for boundary layer micropolar fluid flow. AIMS Math. 2020;5(3):2009-2026. doi:10.3934/math.2020133

[12] Vyas P, Yadav K. EGA for a Convective Regime over a Vertical Cylinder Stretching Linearly. Appl Math Nonlinear Sci. 2021;6(1):515-526. doi:10.2478/amns.2020.2.00058

[13] Monaledi RL, Makinde OD. Entropy generation analysis in a microchannel Poiseuille flows of nanofluid with nanoparticles injection and variable properties. J Therm Anal Calorim. 2021;143(3):1855-1865. doi:10.1007/s10973-020-09919-x

[14] Makinde OD, Eegunjobi AS. MHD FLOW OF A REACTING AND RADIATING NANOLIQUID PAST AN INCLINED HEATED PERMEABLE PLATE: ANALYSIS OF ENTROPY GENERATION. Lat Am Appl Res - An Int J. 2021;51(4):269-276. doi:10.52292/j.laar.2021.715

[15] Vyas P, Khan S, Gajanand. Micropolar couple stress thermofluidics and entropy in Forchheimer channel. Heat Transf. 2021;50(5):4382-4416. doi:10.1002/htj.22080

[16] Eringen AC. Simple microfluids. Int J Eng Sci. 1964;2(2):205-217. doi:10.1016/0020-7225(64)90005-9

[17] Eringen AC. Theory of Micropolar Fluids. J Math Mech. 1966;16(1):1-18. doi:10.1512/iumj.1967.16.16001

[18] Soundalgekar VM, Takhar HS. FLOW OF MICROPOLAR FLUID PAST A CONTINUOUSLY MOVING PLATE. Vol 21.; 1983.

[19] Gorla RSR, Slaouti A, Takhar HS. Free convection in micropolar fluids over a uniformly heated vertical plate. Int J Numer Methods Heat Fluid Flow. 1998;8(5-6):504-518. doi:10.1108/09615539810220261

[20] Kim YJ. Unsteady convetion flow of micropolar fluids past a vertical porous plate embedded in a porous medium.

Acta Mech. 2001;148(1-4):105-116. doi:10.1007/BF01183672

[21] Srinivasacharya D, Ramana Murthy J V., Venugopalam D. Unsteady stokes flow of micropolar fluid between two parallel porous plates. Int J Eng Sci. 2001;39(14):1557-1563. doi:10.1016/S0020-7225(01)00027-1

[22] Kim YJ, Fedorov AG. Transient mixed radiative convection flow of a micropolar fluid past a moving, semi-infinite vertical porous plate. Int J Heat Mass Transf. 2003;46(10):1751-1758. doi:10.1016/S0017-9310(02)00481-7

[23] Kim YJ. Heat and mass transfer in MHD micropolar flow over a vertical moving porous plate in a porous medium. Transp Porous Media. 2004;56(1):17-37. doi:10.1023/B:TIPM.0000018420.72016.9d

[24] Chaudhary RC, Jain P. Combined heat and mass transfer in magneto-micropolar fluid flow from radiate surface with variable permeability in slip-flow regime. ZAMM Zeitschrift fur Angew Math und Mech. 2007;87(8-9):549-563. doi:10.1002/zamm.200610336

[25] Abdulaziz O, Hashim I. Fully developed free convection heat and mass transfer of a micropolar fluid between porous vertical plates. Numer Heat Transf Part A Appl. 2009;55(3):270-288. doi:10.1080/10407780802628961

[26] Das K. Effect of chemical reaction and thermal radiation on heat and mass transfer flow of MHD micropolar fluid in a rotating frame of reference. Int J Heat Mass Transf. 2011;54(15-16):3505-3513. doi:10.1016/j.ijheatmasstransfer.2011.03.035

[27] Sharma R, Kumar Jha A. Heat Transfer in MHD Micropolar Fluid Flow Past a Vertical Plate in Slip-Flow Regime. Mapana J Sci. 2012;11(3):179-191. doi:10.12725/mjs.22.12

[28] Pal D, Talukdar B. Perturbation technique for unsteady MHD mixed convection periodic flow, heat and mass transfer in micropolar fluid with chemical reaction in the presence of thermal radiation. Cent Eur J Phys. 2012;10(5):1150-1167. doi:10.2478/s11534-012-0063-6

[29] Ashraf M, Jameel N, Ali K. MHD non-Newtonian micropolar fluid flow and heat transfer in channel with stretching walls. Appl Math Mech (English Ed. 2013;34(10):1263-1276. doi:10.1007/s10483-013-1743-7

[30] Satya Narayana P V., Venkateswarlu B, Venkataramana S. Effects of Hall current and radiation absorption on MHD micropolar fluid in a rotating system. Ain Shams Eng J. 2013;4(4):843-854. doi:10.1016/j.asej.2013.02.002

[31] Gangadhar K, Vijayakumar D, Chamkha AJ, Kannan T, Sakthivel G. Effects of Newtonian heating and thermal radiation on micropolar ferrofluid flow past a stretching surface: Spectral quasi-linearization method. Heat Transf - Asian Res. Published online 2019. doi:10.1002/htj.21641

[32] Magodora M, Mondal H, Sibanda P. Dual solutions of a micropolar nanofluid flow with radiative heat mass transfer over stretching/shrinking sheet using spectral quasilinearization method. Multidiscip Model Mater Struct. 2020;16(2):238-255. doi:10.1108/MMMS-01-2019-0028

[33] Ahmad S, Nadeem S, Muhammad N, Khan MN. Cattaneo–Christov heat flux model for stagnation point flow of micropolar nanofluid toward a nonlinear stretching surface with slip effects. J Therm Anal Calorim. 2021;143(2):1187-1199. doi:10.1007/s10973-020-09504-2

[34] Rees DAS, Bassom AP. The blasius boundary-layer flow of a micropolar fluid. Int J Eng Sci. 1996;34(1):113-124. doi:10.1016/0020-7225(95)00058-5